ELSEVIER

Journal of Alloys and Compounds 223 (1995) 251–264

Journal of ALLOYS AND COMPOUNDS

Comparison between Ce-monopnictides and An-monopnictides: strong mixing effect

T. Kasuya

Physics Department, Tohoku University, Sendai, Japan

Abstract

The present situation with respect to understanding rare earth and transition metal compounds is reviewed briefly. Ideas essential to the understanding of anomalous heavy fermion rare earth compounds are described in detail by selecting Ce-monopnictides as a typical example. The Kondo state is considered as a typical charge screening mechanism. In the low carrier density systems, the magnetic polaron liquid is shown to play an important role. In general, the unrestricted Hartree–Fock band picture is applicable to the 4f states. General ideas to explain the anomalous heavy fermion U-compounds are presented by borrowing ideas from the 4f and 3d systems. For the anomalous U-compounds, the unrestricted Hartree–Fock picture is proposed to be applicable. Anomalous properties in U-monopnictides and U-monochalcogenides are studied in detail based on the above described ideas, in particular the unrestricted Hartree–Fock picture. It is shown that the main anomalous properties are explained consistently.

Keywords: Ce-monopnictides; An-monopnictides; Rare earths; Transition metal compounds

1. Introduction

The study of rare earth compounds began in the 1950s when the technique to separate various rare earth elements showed remarkable improvement. The first high quality materials obtained were heavy rare earth metals, and various interesting novel transport and magnetic properties were observed, in particular through neutron scattering measurement, a technique newly developed at that time. The essential characteristic that differentiates 4f electrons from 3d electrons is the strong localization, a much smaller radius than those of the 5s and 5p closed shells, and thus a well screened state. The direct f–f exchange interaction between different lattice sites is therefore very weak and the main interaction should be indirect interactions induced through other freedoms. In the heavy rare earth metals, the most important interactions are the intra-atomic 4f–5d and 4f–6s exchange interactions and then, by treating the 5d and 6s electrons as the usual band states, everything including the magnetic and transport properties is governed by the conduction band electrons, in particular a pair of flat Fermi surfaces perpendicular to the *c*-axis causing a strong nesting character. The study initiated by Kasuya [1] and summarized in Ref. [2] became the paradigm for the metallic rare earth compounds.

Eu-chalcogenides, EuXc for Xc = O, S, Se and Te, with a simple NaCl type structure were the first typical non-metallic rare earth compounds to receive intense investigation because high quality single crystals were prepared successfully. Anomalous transport properties, including metal–insulator transition, anomalous magneto-optical properties including anomalous red shift of the absorption peak, and a rich variety of magnetic properties depending on the type of chalcogen and a small doping of carrier were the main attractions; the key concept to explain these anomalous properties was that of the magnetic polaron [3,4]. It was determined that the nearest neighbor, NN, exchange interaction is ferromagnetic and depends strongly on the Eu–Eu distance, while the next nearest neighbor, NNN, exchange interaction through the chalcogen, Eu–Xc–Eu, is the usual antiferromagnetic superexchange interaction. The origin of this unusual ferromagnetic exchange interaction was attributed to the following mechanism [5]: a 4f electron on the central Eu atom mixes with the same f-symmetry wave function formed mainly by the 5d states on the NN Eu sites and this 5d electron aligns the 4f spins on the NN Eu through the intra-atomic d–f exchange interaction. Indeed, this mechanism could explain the strong Eu–Eu distance dependence very well. In optical absorption, a 4f electron at the central Eu is excited to a 5d state in the same Eu

SSDI 0925-8388(94)09013-0

atom. This is a typical intra-atomic f–d exciton and this 5d electron extends on the NN Eu sites and polarizes their spins, or is subject to the d–f exchange field when these Eu spins are aligned ferromagnetically. This is the origin of the anomalous red shift of the f–d magnetic exciton [6,7]. When one 5d electron is created by doping, it polarizes the surrounding Eu spins through the d–f exchange interaction and is trapped in this exchange field. This is the self-trapped magnetic polaron, similar to the self-trapped phonon polaron studied before by Landau (see Ref. [8] and references therein). However, the magnetic polaron is much more complicated and shows various novel properties because the spin polarization depends strongly on temperature T, magnetic field H, and pressure P (see, for example, Ref. [9] and the references in Ref. [10]). In particular, it shows a critical fluctuation effect near the magnetic ordering temperature. In EuXc, however, carrier doping was done by substituting Eu by a trivalent rare earth atom R^{3+} such as La or Gd, or by chalcogen defects, obtaining a defect-trapped magnetic polaron or magnetic impurity state, where the main binding force is impurity potential. These trapped magnetic polarons cause various anomalous transport properties including a metal–insulator transition. The above-mentioned studies were performed mainly by Kasuya and the experimental group at IBM as a collaborative work [11].

The impurity Kondo problem was first studied on a 3d transition metal impurity such as Ni, Fe and Mn in, for example, Cu. In these systems, however, the impurity concentration must be very low, much less than 1%, to obtain the real impurity Kondo effect because strong magnetic interaction between impurities destroys the impurity Kondo effect very easily (for a review see Ref. [12] and references therein). From early 1970, however, the dense Kondo effect, or more generally the valence fluctuation phenomena causing heavy fermion characteristics, was found in several rare earth metallic compounds, in particular in Ce and Sm compounds, and attracted much attention. In the rare earth compounds, in general, the intersite magnetic interaction is weak and thus even in 100% pure rare earth compounds the impurity Kondo effect is observed at high temperature. At low temperature, however, because of crystalline perfection, the Kondo states form a kind of coherent state, called heavy fermion, which shows various anomalous behaviors, such as a gap state, called the Kondo insulator, anomalous superconductivity and various unusual magnetic states caused through competition between the Kondo state and the intersite magnetic interactions. In the low carrier systems, the long-range Coulomb interaction becomes dominant and thus the competition with the Wigner crystal formation supported by the magnetic polaron formation mentioned above becomes the main problem. Even though there are still many unsolved problems on the above anomalous properties, we have a qualitative understanding of the fundamental characteristics, in particular for the Ce and Yb compounds. A more detailed description will be given in the next section.

The study of the 3d transition metal compounds, in particular of the magnetic metals such as Ni and Fe, has a long history and we know now that at least for the typical metallic magnetic materials the usual 3d band model can be a good starting base for a detailed investigation. Indeed, the Fermi surface observed by the de Haas van Alphen effect, dHvA, is well reproduced by the band calculation [13] and the spin wave dispersion is reproduced very well by the dynamic magnetic susceptibility $\chi(q, \omega)$ calculated through the band model [14]. Optical properties, such as angle-resolved photoemission spectra, ARPES, detecting the band states below the Fermi energy E_F, are also consistent with the band model including some modification due to interaction and lifetime broadening [15]. In contrast, in some insulator magnetic systems, an approach from a localized picture similar to that in the rare earth compounds is applicable. In the high T_c materials of the layered CuO_2 type, a typical low carrier density system, similar to some low carrier density rare earth compounds such as the Ce-monopnictides, CeXp, Xp = N, P, As, Sb or Bi, is pointed out [16]. This will be treated in more detail in the next section.

Compared with the above-mentioned 4f and 3d systems, studies of the 5f system are scarce even for the most common materials, the U-compounds. However, study of these 5f systems is very interesting and very important for the fundamental physics of the electronic structure because in U the 5f state is more extended than the 4f state, but still situated inside the 6s and 6p closed shells and thus much more localized than the 3d state, that is, in between the 4f and 3d states and thus connecting these two systems. Therefore, the U-compounds are really situated in between the localized and the itinerant states and various novel properties are expected for materials at the boundary. Indeed, the U-compounds belonging to such a boundary region show various novel anomalous properties. Some of them seem to be similar to, but not the same as, the heavy fermion character in rare earth compounds. The clearest difference is seen in PES and IPES, inverse photoemission spectra, or BIS, in which no essential difference exists between the typical heavy fermion system and the typical 5f band system, a good typical metal, as well as a well localized normal magnetic system [17]. This characteristic is one of the most important clues in solving the mysteries of the U-compounds.

In the following, we discuss actinide monochalcogenides and monopnictides, AnXc and AnXp, because they have the simple NaCl type crystal structure, suitable for theoretical treatment, and have been investigated

most extensively among the U-compounds. Furthermore, their counterparts, RXc and RXp, have also been investigated most extensively among the rare earth compounds both experimentally and theoretically, and in particular for CeXp even quantitatively, and we now understand the fundamental mechanisms for their anomalous properties. Anomalies in AnXp are substantially different from those in CeXp but similar in some fundamental characteristics. This suggests that even though the situation in AnXp is much more complicated than that in CeXp, the fundamental mechanism is the same and thus modification and extension of the mechanism in CeXp may be applicable to solve the problem in AnXp, as well as in AnXc. In the next section, the situations in RXp and RXc are summarized. In Section 3, a fundamental model of the An compounds is discussed in comparison with that of rare earth compounds. In Section 4, the model is applied to UXp and UXc. For reasons of space we concentrate mainly on UXp.

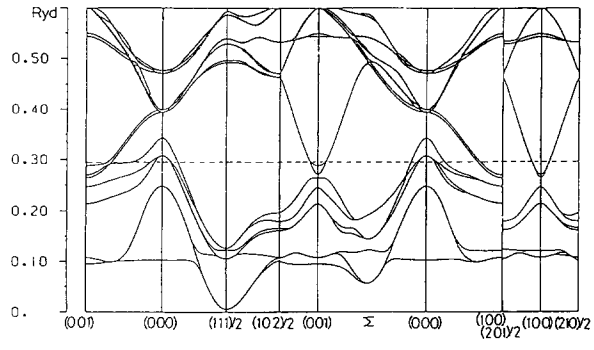

Fig. 1. Band calculation of CeSb for the ferromagnetic ordering in which one 4f state with $j_z = 5/2$ is set below the Fermi energy, seen as a flat band at $E = 0.10\ R_{yd}$. The top of the valence band is at $E = 0.34\ R_{yd}$ on the Γ-point (000). This is the special Γ_8 state mixing strongly with the occupied 4f state and thus pushed up by $0.034\ R_{yd}$ from other Γ_8 states. The Γ_6 doublet is split by the spin–orbit interaction and is situated further below the Γ_8 states. The bottom of the conduction band is at each X-point split by anisotropic d–f exchange interaction. At the Γ-point, the 5d t_{2g} and e_g states are split due to the crystal field effect with the t_{2g} state lower.

2. Summary of mechanisms in rare earth compounds

For the sake of brevity, we will concentrate on the mechanisms in CeXp. It is now well established that there are two well separated regimes in Ce and Yb compounds. Because the situation in Yb can be understood from that in Ce via electron–hole symmetry, we will mainly discuss the Ce-compounds. In the first regime, the Fermi surface can be reproduced very well by the usual 4f band model, similar to the metallic 3d systems, and this regime is called the valence fluctuation regime [18]. Even in this regime, some materials show a fairly strong heavy fermion character. For example, in $CeRu_2Si_2$, the γ-value, the coefficient of the T-linear specific heat at low temperature, is more than 300 mJ $mol^{-1}\ K^{-2}$ and the effective mass is enhanced by more than 100 times. Such a material is situated close to the boundary between two regimes and thus has strong low-frequency spin fluctuation. The strong mass enhancement is due to this spin fluctuation, essentially a similar singularity effect at the Fermi surface as in the electron–phonon interaction case.

For a material in the Kondo regime, one 4f electron is below the Fermi energy and thus the other 13 states are above the Fermi energy separated by the effective 4f correlation energy U_f. Therefore, this situation corresponds to the unrestricted Hartree–Fock model, URHF [18]. The conventional band calculation using the local density approximation, LDA, cannot handle URHF. Therefore, a more flexible method should be used [19]. Then the Fermi surface of CeSb can be reproduced very well by this type of URHF 4f band model, as shown in Figs. 1 and 2 [19,20]. In the Kondo regime, however, the band picture, or the quasiparticle picture, is applicable only very near the Fermi energy, markedly different from that of the 3d metallic systems mentioned before. This difference stems from the following fact. In the 3d systems such as Ni and Fe, the intra-atomic d–d Coulomb interaction is strongly screened by the 4s–3d Coulomb interaction and thus the effective d–d correlation energy U_d in the metallic crystal is small, less than 2 eV, or about 1 eV in Ni and Fe while the 3d bandwidth is more than 3 eV, causing the 3d band picture to be fairly good. In the 4f systems, the screening by the 5d electron is not sufficient and thus the effective f–f correlation energy U_f is large, typically about 7 eV in the Ce-compounds. Conversely, the 4f bandwidth, which is caused through c–f mixing, is about 1 eV, as seen in Fig. 1. Therefore, fundamentally, the atomic many-body character is kept well even in metals. Indeed, the 4f PES and BIS spectra show a clear atomic structure based on the LS coupling scheme. Therefore, the quasiparticle picture is applicable only very near the Fermi surface. As shown by Luttinger [21], as long as the perturbation with respect to the Coulomb interaction does not diverge, the Fermi liquid model with quasiparticles is applicable at least near the Fermi energy, where the inverse lifetime of the quasiparticle τ^{-1} increase proportionally to $(E-E_F)^2$. This means also that τ^{-1} is proportional to T^2, and the charge fluctuation is weak near the Fermi energy. In contrast, because the local magnetic moment is strong, there is strong low frequency spin fluctuation. Owing to this strong fluctuation, τ^{-1} increases linearly with $E-E_F$ and T except very near E_F, destroying the quasiparticle, and the effective mass is enhanced strongly at E_F. This is often called the decoupling of spin-charge fluctuations.

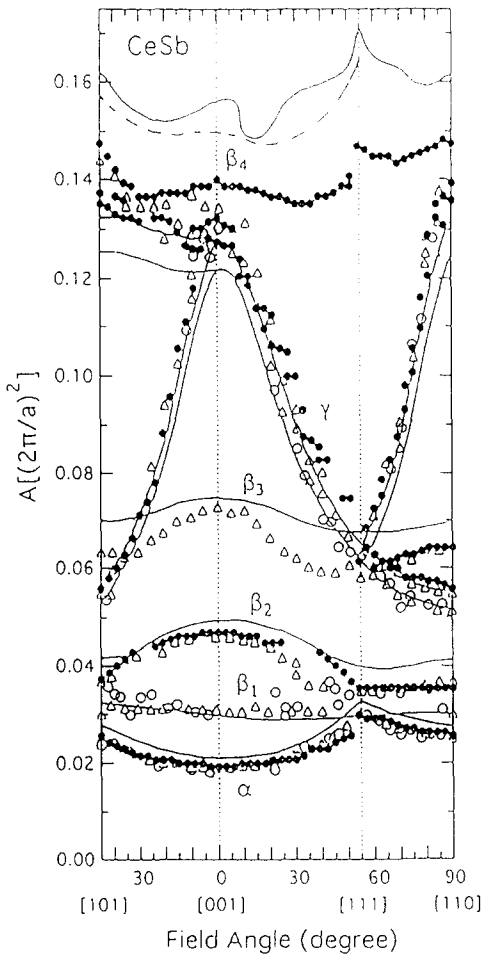

Fig. 2. Observed Fermi surface cross-section A is shown by open and closed circles and triangles, while the calculated results are shown by solid lines. The dashed line is the result of an improved calculation. The β_4 branch corresponds to the hole surface particularly pushed up by the occupied 4f state through the p–f mixing effect, as shown in Fig. 1.

The high-frequency phenomena should therefore be explained with local picture. A typical example is seen in the measurement of the occupied 4f level. We cannot observe the 4f level within the ground state. The most common and unique method to observe the occupied 4f level spectra is resonance 4f PES, in which a 4f electron is excited out and the final state energy spectrum is observed. This is the physically observable occupied 4f level spectrum in many-body systems. In the final state, the created 4f hole is screened in various ways and there are two main screening processes, the bonding and antibonding c–f Kondo screenings, and then a two-peak structure appears as shown in the following.

The usual model of charge screening in metals is the conventional one-particle band picture, that is, to solve the one-particle state self-consistently including the potential of the created hole [22]. This is, however, not the true screening state because of the lack of the many-body effect due to the Coulomb interaction between the conduction band electrons. Indeed, the bare intra-atomic 5d Coulomb energy, U_{dd}, is as large as 10 eV. When U_{dd} is very large, the screening is done by one 5d electron because this is the best way to avoid U_{dd}. The real situation falls between the above two limiting cases. A typical example of charge screening occurs when a core electron is removed from the central Ce atom. Then we have the core X-ray photoemission spectra, core XPES. This is a typical high-frequency phenomenon because the created core hole is filled very quickly causing a large lifetime broadening in each peak. Because of the high-frequency process in the sense mentioned above, the phenomenon is very local and the electron cannot go beyond the NN sites. Then a typical 5d screening is given by the p–d bonding Kondo state given in the zeroth approximation by

$$(\alpha_0 + \sum_{\mu} \alpha_\mu c_{d\mu} d_\mu^{+})|0> \quad (1)$$

for the case of CeX, for example, where d_μ^{+} is the creation operator of a 5d state of μ-symmetry on the central Ce atom, $c_{d\mu}$ is the annihilation operator of the band electron of d_μ symmetry formed mainly from the p-states on the NN X-sites and α_0 and α_μ are numerical parameters. The real situation is more complicated [23] and Eq. (1) is a simplified form for the bonding p–d Kondo state. In the p–d antibonding Kondo state, the sign of α_μ changes. In the typical bonding and antibonding Kond states, the charge neutrality is kept very well, indicating that the core hole charge is nearly completely screened by the 5d electrons [23]. There are many other higher energy screening states, in which the charge neutrality is no longer satisfied, but their probabilities are small and thus are not well observed. In the case of the core spectra at X, however, the second excitation peak is also observed in agreement with the calculation [23]. Because of the much larger value of p–d mixing compared with p–f mixing, the energy splitting between the p–d bonding and antibonding Kondo states is estimated to be about 10 eV in CeX, in good agreement with the experimental result.

It is also possible to screen the core hole charge through the 4f electrons with a lower screening energy. As mentioned before, the effective 4f correlation energy, 6 eV, means that the 4f screening energy may be about 6 eV lower than that for the 5d electron. Indeed, the calculation including both the 5d and 4f screening shows that the peak of the p–f bonding Kondo screening is about 5 eV below that of the p–d bonding Kondo screening [23]. Therefore, this is the best screened peak. However, because the p–f mixing is much weaker than the p–d mixing, and is therefore the slower process, the former best screened peak is observed only as a shoulder of the 5d screened main peak, again in good agreement with the calculation. Note that the peak intensity is proportional to how much the final state

is included in the initial ground state. Because of the larger p–d mixing, this amount is much larger for the d-screening peak in which one more 5d electron is included. Note also that the p–f antibonding Kondo screening peak is about 2 eV higher than that of the p–f bonding Kondo peak and is thus not clearly separated from the main peak. This is discussed below. It is also important to notice that because the p–d fluctuation is much faster than the p–f fluctuation, the latter is screened very well by the p–d charge polarization. Therefore, in the p–f bonding Kondo state, the α_0 term in Eq. (1) is written as $\Sigma_\mu \alpha_\mu c_{d\mu} d_\mu{}^+$, or when this part is included in the background state $|0>$, the p–f bonding Kondo state may be written in its simplest form as

$$(\alpha_0 + \sum_{\nu\mu} \alpha_{\nu\mu} d_\mu c_{d\mu}{}^+ c_{fv} f_v{}^+)|0> \quad (2)$$

This means that during the 4f charge fluctuation the charge neutrality is always kept. For the core PES, the p–f Kondo electron or hole with f_v symmetry is nearly localized on the NN sites. As the lifetime of core hole becomes longer, the Kondo electron, or hole, extends more from the central site. In the quasistatic phenomena, we obtain the usual Kondo state, extending well over the crystal using the band states near the Fermi energy. Therefore, the Kondo state should be recognized as the ground state for the charge screening of the 4f charge fluctuation.

Now we come back to the resonant 4f PES. For CeXp, as an example, at the center site Ce under consideration, the $4f^0$ state is created and the best screening of the 4f hole is achieved by the p–f bonding Kondo state. The peak p–f bonding Kondo state changes from 1.2 eV to 0.8 eV as Xp changes from Bi to P accompanied with increasing intensity, as shown in Fig. 3. This is because the effective 4f level, that is, the 4f hole screened by the 5d electrons as described above, approaches the Fermi energy with increasing strength

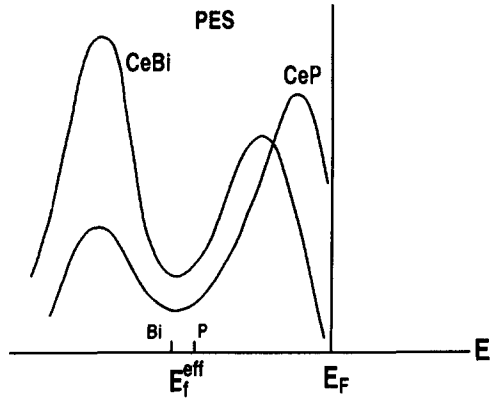

Fig. 3. Schematic picture of the 4f resonance photoemission spectra for CeBi and CeP. The position of the effective 4f level, well screened by the 5d electron, E_f^{eff}, is shown by bars. The p-valence band exists from E_F to the deeper 4f peak position with the peak near E_f^{eff}.

of p–f mixing as Xp changes from Bi to P and in CeN the p–f bonding Kondo peak crosses the Fermi energy causing CeN to enter the valence fluctuation regime, a monovalent metal with the 4f band model. This sudden shift of the peak in CeN is mainly due to sudden increase in the 5d–4f mixing interaction between the NN Ce atoms because of the shortened Ce–Ce distance in CeN, which is further enhanced by a substantial reduction in the lattice constant because of the metallic bonding. Conversely, the p–f antibonding Kondo peak sits about 2 eV deeper than the p–F bonding Kondo peak mentioned above, whereas a broad p–d antibonding Kondo peak is expected at around 10 eV below the Fermi energy. However, because it is a broad peak, in practice it is difficult to separate it clearly from the background, which is strong in this energy region. As described above, PES and BIS give very important information on the 4f state and later very different behavior of the 5f state is shown to clarify the difference between them. Note that when one 4f electron is removed from the initial state, the effective 4f level, well screened by the 5d electron as mentioned before, sits near the center of the p-valence band and thus is split into the bonding and antibonding p–f Kondo state in the sense described in Eq. (2). In the usual treatment of the p–f Kondo model, the 5d states are not considered explicitly but are treated so as to screen the 4f hole, immediately causing the effective 4f level. This is approximately correct to explain the low-energy part of the 4f PES but not correct to explain the core PES [23].

It was shown before that for the 3d metal systems such as Ni and Fe the 3d band model is good in the first approximation, even in the entire 3d band region. However, even in these systems, a many-body satellite peak appears, for example at 6 eV below the Fermi energy in Ni [24]. This is interpreted to be a type of s–d antibonding Kondo peak for the following reason. As stated before, the 3d hole is effectively screened by the 4s state and thus in Ni the following three configurations exist in nearly equal proportions: $3d^{10}$, $3d^9 4s$, $3d^8 4s^2$. However, the $3d^7$ configuration cannot be screened by 4s sufficiently because only a $4s^2$ configuration is possible. Therefore, when one 3d electron is removed from the $3d^8 4s^2$ configuration, the screening mechanism is substantially different from the other two cases. In the case of the first two configurations, the created 3d hole is immediately screened by the 4s electrons through the most efficient screening process, and then we obtain the usual 3d band state made from the above three configurations. For the last configuration, because the most efficient 4s screening does not work, the s–d bonding and antibonding Kondo screenings become effective. Because of the small effective correlation energy, the s–d bonding Kondo state relaxes to the usual 3d band state, but the s–d anti-

bonding Kondo state is much deeper than the 3d band state and thus remains as a localized state. This is the 6 eV satellite peak. It is often claimed that the deep satellite peak in Ni means a fairly strong d–d correlation. The above picture indicates that the effective d–d correlation depends strongly on the 3d–4s configuration due to the limit of double occupation of the 4s states and the 3d band model is well applicable within the above-mentioned three kinds of d–s configuration. In the 5f electron case, the 6d electrons are the main screening charge, and thus there is practically no limitation of the type mentioned above for the screening by s-electrons. Except for this point, however, the situations in the 3d and 5f cases are similar in the sense of a weak correlation.

Recently, low carrier strongly correlated systems have attracted much attention because the high T_c CuO_2 layered systems belong to this category as a typical example of the 3d systems. In the 4f systems, RXp are the most typical example because high-quality single crystals have been prepared giving detailed information on the Fermi surface, which is crucially important to understand the fundamental electronic state. Moreover, similarity between the above two materials has been stressed by the present author [20,25,26]. There are two main problems for low-carrier 4f systems. First, even in low carrier density systems, typical Kondo behavior with the value of T_K being of the order of 10 K is observed. As particularly stressed by Nozier, people wonder why a small number of conduction band electrons with energies within T_K from the Fermi energy can make all the 4f systems singlet. This puzzle is further enhanced in the low carrier density systems. Moreover, the observed value of T_K mentioned above is many orders of magnitude larger than that calculated as the impurity Kondo problem, which is very small because of the low density of state at the Fermi energy. Second, it is well known that in the limit of low carrier density the long-range Coulomb interaction overcomes the kinetic energy and thus a kind of electron lattice, called a Wigner crystal with strong quantum fluctuation, is formed. Owing to strong zero-point vibration, Wigner crystals melt easily and form a kind of liquid with strong local correlations. We call it a Wigner liquid, and it is expected to exist in a wide range of ratios of Coulomb and kinetic energies. In the 4f system with a 4f magnetic moment, magnetic polarization is induced in the Wigner crystal. In exactly the same but a much clearer sense than the doped low carrier systems studied before, two kinds of magnetic polaron systems are expected. One is the case where the localization through the Coulomb repulsion is dominant and then the magnetic polarization is induced on the Wigner crystal. This case may be called a magnetic Wigner crystal, or weak magnetic polaron crystal. When the self-trapped localization due to the magnetic interaction is dominant, the localization range is determined primarily by each magnetic polaron itself. As studied before for the doped systems, this polaron is usually the strong polaron in which a nearly full magnetic polarization is achieved within each polaron. Therefore, the localization range is primarily determined by this condition. The structure of the magnetic polaron lattice is primarily determined so as to minimize the energy of the electronic state. Examples are shown later for CeXp.

In the Wigner liquid state, too, when the motion of the charge, or spin, density is slower than a typical lifetime for the 4f spin polarization τ_m, local magnetic polarization is induced, enhancing the localization character of the Wigner liquid. We call this state a magnetic polaron liquid. Then, the motion of the magnetic polaron liquid is determined primarily by τ_m, which may be a local longitudinal relaxation of the magnetic moment or spin wave velocity [9]. Therefore, we are interested in whether such novel states are actually realized in CeXp, the best quality materials we can obtain at present, because the magnetic polaron liquid and lattice are very easily destroyed by any defect, and change to the trapped magnetic polaron or magnetic impurity state mentioned before. Then, a complicated effect of randomness governs the anomalous properties and thus the intrinsic characteristics for the magnetic polaron are difficult to observe.

Indeed, in CeXp we could observe the magnetic polaron liquid and lattice [20,27]. In CeP and CeAs the magnetic polaron liquid is observed even at room temperature. In these materials the ground crystal field level is the Γ_7 doublet and the excitation energy of the Γ_8 quartet is about 170 K. As shown before, only Γ_8 p–f mixing is possible because the valence bands have only Γ_8 and Γ_6 states at the Γ-point and its matrix is more than 10^4 K [28]. The carrier number at room temperature is about 0.015 per Ce and thus each polaron extends over about 100 Ce sites because at this temperature the induced moment is weak and thus the Coulomb repulsion is the main localization force. Then each polaron expands as much as possible until the overlap among polarons becomes substantial. It is then evaluated that within the v-th hole polaron, the v-th Γ_8 4f state is pulled down through the p–f mixing interaction by as much as nearly 100 K. In this situation, the magnetic polaron rapidly becomes weaker as the temperature decreases beyond 100 K, accompanied by a decreasing carrier number. Note that an electron–hole pair is created to form a magnetic polaron as far as its formation energy gain is larger than the necessary energy to create an electron–hole pair [29]. At low temperatures, supported further by applied magnetic field and applied pressure, the weak magnetic polaron changes to the strong magnetic polaron with nearly full moment. In CeP, such a transition occurs at 10 K under an applied magnetic field of 1 T, while in CeAs

it occurs under a magnetic field of 12 T, or an applied pressure of 1 GPA [30]. In CeP, the carrier number at low temperature including the above-mentioned ordering state is about 0.008 per Ce, less than half that at 100 K. To bring down a particular $4f\Gamma_{8\nu}$ state sufficiently below the ground $4f\Gamma_7$ state, the ν-th Γ_8 p–f mixing effect on each Ce site within the magnetic polaron should be on the order of 300 K and then the extension of the magnetic polaron should be as small as to cover about 25 Ce atoms. By multiplying the carrier number mentioned above, the ratio of volume covered by the strong magnetic polaron, or the ratio of the $4f\Gamma_8$ state to the $4f\Gamma_7$ state outside the polaron, is evaluated to be about 0.2. This is indeed obtained from neutron scattering measurements [31], as well as from magnetization measurements [32]. The 4f state with full moment extends on the plane perpendicular to the moment because this is the best way to obtain full p–f mixing with the NN Xp atoms. Therefore, the strong magnetic polaron lattice becomes a layered type with the aligned moment perpendicular to the layer. Neutron scattering measurements revealed the 11-layer period of double Γ_8 layers. The 11-layer period is consistent with the RKKY type period through the Fermi wave vector $\boldsymbol{k}_{F0}$ of the electrons at the X_x and X_y points. This means that the holes and the X_z electrons with wave functions extending on the x–y plane are mostly localized on the double Γ_{80} layer for the p–f mixing and charge neutrality, respectively, and the electrons around X_x and X_y points are nearly uniformly distributed due to their small effective mass m_z but are perturbed by the 11-layer period which is consistent with k_{Fz}, where Γ_{80} means the 4f state of full moment along the z-axis. All the anomalous properties are explained consistently by this magnetic polaron model.

Even in the case where the magnetic polaron liquid is not formed, the Kondo electron created by the c–f mixing is more localized in the low carrier density system than in the typical metallic system because of the positive charge left near the central site, which is not well screened in the low carrier density systems. The amplitude at the NN sites increases, causing stronger p–f mixing and thus a larger value of T_K. Indeed, the large value of T_K in CeSb mentioned before can be explained by this mechanism [33].

When the above mechanism becomes stronger, the Kondo electrons become really localized, forming the localized Kondo singlet state, in contrast to the usual metallic case. This is particularly enhanced when the Luttinger theorem predicts an energy gap. SmB_6 and YbB_{12} are typical of materials that belong to this category and are called Konto insulators [34,35]. Recently various Ce-compounds have been found to belong to this category.

3. Fundamental characteristics of the 5f state

As mentioned before, the effective 5f–5f correlation energy U_f in U-compounds is small, typically 1–2 eV in most compounds, and thus the situation is rather similar to the 3d state even though the main part of the 5f state is well screened by the 6s and 6p closed shells, in contrast to the 3d state, which is situated mostly outside the 3s and 3p closed shells. Indeed, many metallic U-compounds are well described by the usual 5f band model, with the Fermi surface well defined by this model with a weak mass enhancement. In such materials, PES and BIS are also well modeled by the band model as shown typically in Fig. 4. The 5f band model is calculated based on the j–j coupling scheme, in which $j=7/2$ states have about 1 eV more energy than $j=5/2$ due to the 5f spin–orbit interaction. Therefore, $j=5/2$ bands are observed in PES mainly less than 1.5 eV below the Fermi energy. Some $j=5/2$ bands are also observed in BIS just at the Fermi energy, forming a shoulder, and the $j=7/2$ bands form a peak in BIS at about 1.5 eV above the Fermi energy, extending to about 2.5 eV above the Fermi energy. The result of the band calculation can fit the experimental result very well, in particular for the case of weak mass enhancement [18]. Therefore, the problem lies in the cases of heavy fermion and well localized regimes. Note that, in contrast to the case of Ni mentioned before, there is no marked satellite peak at higher energy either for PES or BIS. This confirms the model proposed before, that the 6 eV satellite in Ni, which is also common in the 3d compounds, is a special characteristic of the 4s screening in which only configurations up to $4s^2$ are possible.

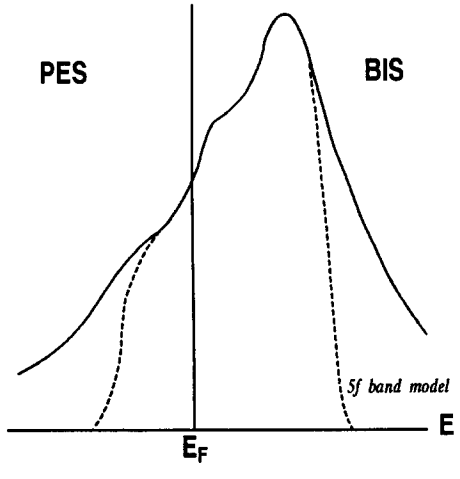

Fig. 4. Schematic pictures for the 5f PES and BIS in the U-compounds. The dotted curve corresponds to the result of the usual band calculation and also to the experimental result for a good normal metal while, the solid line corresponds to the heavy fermion U-compounds.

It is well established that the main feature of PES and BIS described above does not change even in the anomalous U-compounds in the heavy fermion regime. The main difference is the larger tails in both PES and BIS, enlarged with increasing character of localization, and thus largest for materials in the well localized 5f regime such as UPd_3 and UBi [36]. At low temperature, a sharp peak appears at the Fermi energy. This peak is seen only in a measurement with high resolution [37]. In materials of well localized regime, a pseudo gap opens at the Fermi energy [36]. The above facts indicate clearly that the 5f band model is still a good starting point for understanding anomalous behaviors in heavy fermion U-compounds because of the small value of U_f even for the heavy fermion systems, including the localized moment regime. The large tails in PES and BIS are clearly due to the stronger correlation effect but are still not strong enough to cause an antibonding Kondo peak, such as observed in rare earth compounds. Note that the antibonding Kondo peak is often misunderstood as being due to the usual antibonding state. As described in detail before, this is clearly due to the Kondo state, like the many-body state for the system with strong correlation, and thus no such peak appears in the U-compounds with weak correlation energy U_f even in those of heavy fermion and localized regimes. In the case of U-compounds, the tail is formed by a series of states with various $5f^n$ configurations. As the 5f correlation increases, intensity for each peak increases and the energy distance between two configurations increases, causing more extended tails for both PES and BIS, in good agreement with the experimental facts.

Compared with Ce-compounds, where $4f^0$ and $4f^1$ are the main configurations, U-compounds have many $5f^n$ configurations, where n is mainly 2 or 3 but terms with larger n values are also not negligible due to a small U_f value, and thus another problem of how to treat the many-5f intra-atomic state exists. It is well known that for the light actinide atoms the LS coupling scheme is better than the j–j coupling scheme, at least for the ground configuration. In crystals with strong c–f mixing, however, the situation is more complicated, in particular in the heavy fermion regime. Measurement of the form factor by the polarized neutron scattering gives the most detailed information for the coupling scheme, including the value of n, and the results of band calculations are encouraging, even though a more sophisticated treatment is necessary [38]. Even though the band calculations start from the j–j coupling scheme, the orbital moment is reduced substantially through the strong c–f mixing interaction and thus approaches the LS scheme. In this sense, this is called an intermediate coupling scheme [38]. Therefore, also in this sense, the band model gives a good starting point. In the magnetic ordering state, as well as in the anomalous compounds, the unrestricted Hartree–Fock picture, the same model as in CeSb described before, should be applicable. However, because more than two 5f states are occupied and their c–f mixing intensities are different, the situation is more complicated. In the next section, we shall treat UXp and UXc from the above standpoint, and study how this can explain various novel anomalous properties in these materials.

4. Mechanisms of anomalous properties in UXp and UXc

From various experimental observations, U in UXp is thought to be primarily trivalent, similar to Ce in CeXp [38]. To apply the Luttinger theorem, this is very important because in this case three 5f states should be put below the Fermi energy and the Fermi surface should be determined based on this configuration. Semimetallic behavior results, with some amount of holes and electrons, similar to that described before for CeSb, even though the real band structure may be much more complicated owing to the large number of occupied 5f states and to stronger p–f mixing interaction. The valence and conduction bands formed by p(Xp) and 5d(U), as well as the orthogonal plane waves, OPW, should be essentially the same as those of LaXp shown in Fig. 1 when the p–f mixing effect is omitted. Then three 5f states should be put below the Fermi energy. It is reasonable and convenient to treat the 5f bands by using the tight binding model assuming the atomic 5f states. This is also important in the 3d systems. Indeed, the magnon dispersion in Ni and Fe can be calculated correctly only by using the tight binding 3d bands and OPW [14]. While the total energy is not sensitive to the wave function, the dynamic properties are much more sensitive to it, and thus give important information on the latter.

The band model is applicable in principle to the ground state, and thus we should treat the magnetic ordering. There are two kinds of fundamental ordering. One is essentially the same as those in CeXp, the ferromagnetic layer on the xy plane with the moment along the z-axis and a simple antiferromagnetic ordering along the z-axis. This is called $1\boldsymbol{k}$ type I ordering. Another is $3\boldsymbol{k}$ type I ordering in which three types of the above ordering with $\boldsymbol{k}_x$, $\boldsymbol{k}_y$ and $\boldsymbol{k}_z$ coexist. Other types of ordering are understood as modulations from the above two fundamental forms [39]. Therefore, in the following, these two fundamental orderings are studied.

A natural way to choose three orthogonal occupied 5f states is the combination of one that is the same as that in CeXp with the full moment and the full p–f mixing called Γ_{8O}, and two others causing the lowest intra-atomic Coulomb-exchange interaction with the first

one. Because the unoccupied 5f states with j = 5/2 sit very near the Fermi energy, the p–f mixing effect is very strong causing a large crystal field splitting between the ground Γ_7 and the excited Γ_8 states of the order of a few thousand degrees k. Therefore, the above two states are fundamentally of the Γ_7 character with induced moments through the intra-atomic Coulomb-exchange interaction with the occupied Γ_{80} state. It is well known in the atomic Hartree–Fock calculation that the unoccupied 5f state has a more extended wave function than the occupied 5f state, because of the weaker attractive potential due to one more 5f state. This means that the Γ_{80} state is more extended than the other two. Owing to strong p–f mixing, its occupation number decreases substantially and moreover it sees an attractive potential at the NN Xp sites. Note that the decreasing 5f population through the mixing from the occupied 5f states is well compensated by the mixing to the unoccupied 5f states and thus the average valence is kept at about three in the present case. Because of the above situation, the 5fΓ_{80} state sits near the top of the valence band and the strong p–f antibonding Γ_{80} band is pushed up above the Fermi energy much more strongly than in CeXp. In the case of normal metals in which the density of states and the c–f mixing strength is nearly constant around the Fermi energy, the energy gain E_m due to the above situation is proportional to the square of the 5f moment, M_f^2. We call this the linear relation. In the low carrier density systems such as CeXp and UXp, the density of states increases strongly with increase in $|E - E_f|$. We call this situation the non-linear relation. As showing in Fig. 1, the dispersion of the antibonding Γ_{80} band along the Γ–X_z axis is weak and thus when the Γ_{80} band rises above the Fermi energy at X_z, the density of states becomes nearly constant due to the two-dimensional character of the system. The p–f mixing is strongest at the Γ-point and becomes weaker as k deviates from the Γ–X_z axis. Therefore, the negative non-linear relation is expected beyond the above situation. This situation is shown in Fig. 5. As shown in Fig. 1, CeXp is very near the critical situation, M_{fm}^2, and UXp is thought to be far above the critical situation. It is important to notice that because the unoccupied 5f states are closer to the Fermi energy than the 4f states, the valence p-bands of UXp are pushed down substantially more than those of CeXp. However, in the 6d systems, the overlap with the valence band is larger in general than that in the 5d systems. Therefore, the 1k state is unstable for UXp because it is better to divide the moment into three independent components, M_x, M_y and M_z. This is the 3k type I structure. The main mechanism to stabilize the 1k structure is thought to be the magnetoelastic effect. In CeSb the c-axis shrinks in the 1k structure [40]. This is thought to be due to the following mechanism. To gain the crystal electric field energy

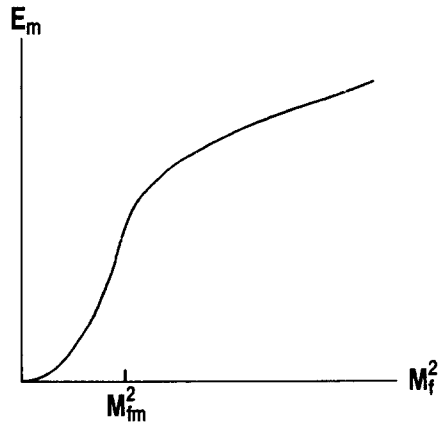

Fig. 5. Schematic picture for the magnetic energy E_m as a function of the square of the magnetization M_f^2. The value shown by M_{fm}^2 corresponds to the steepest point, indicating the crossover from the positive non-linear region to the negative non-linear region.

for Γ_{80}, the c-axis shrinks and the ab-axis expands. To gain the p–f mixing energy, the ab-axis should shrink. However, to gain the p–f mixing energy with the unoccupied 4fΓ_8 states, the opposite distortion is required. Because the unoccupied 4f levels are 5 eV above the Fermi energy, this effect is weak. To preserve the total volume, the c-axis shrinks, but the change in the ab-axis is small. In the 1k structure in UXp, the crystal electric field has a more important role than that in CeXp because the quadrupolar moment of the 5f state is much larger than that in the 4f state. However, the p–f mixing in UXp is stronger than that in CeXp but not by much, less than a 40% increase. Furthermore, the unoccupied 5fΓ_8 is very close to the Fermi energy. As a result, a similar but more enhanced uniaxial distortion is expected in the 1k structure. This is actually observed in the 1k structure in NpAs [39], which shows similar behavior to UAs. Such a uniaxial distortion is not observed in the cubic 3k structure. In the cubic structure, a large volume expansion is observed both in USb and NpAs [39], contrary to the double k structure in the low-temperature phase of UAs. This is definitely opposite to a gain in the crystal field energy as well as the p–f mixing energy. The cause of the volume expansion, 1.2% in USb and 0.4% in NpAs, is an increase in the localized moment, similar to the 3d compounds. Because the increase in the localized moment is larger than the decrease in the p–f mixing matrix, the total energy gain is achieved in the p–f mixing effect. This means that with decreasing p–f mixing, the local 5f moment increases more strongly than the decreasing ratio of the p–f mixing. Therefore, in the 1k and 3k structures, the crystal distortions are quite different. It is difficult to evaluate which one has the stronger energy gain. The energy gain for the 1k case is expected to be larger than that for the 3k case at higher temperature.

The simplest way to obtain the 3*k* structure is to put three 5f states with full moments along the x, y and z axes, that is Ψ_x, Ψ_y and Ψ_z, below the Fermi energy. These states are, however, not orthogonal to each other and the simplest way to make an orthogonal set within them is to rewrite them as

$$\Psi_z - \alpha(\Psi_x + \Psi_y) \text{ etc.} \quad (3)$$

in which $\alpha = \{1+\beta-(1+\beta-2\beta^2)^{1/2}\}/(1+3\beta)$ and α is approximated by $\beta/2$ for a small value of β, where $\beta = (\Psi_x|\Psi_y)$. Of course, a better variational function gives a better result. In particular, because Γ_7 is the ground state, the Γ_7 character should be added. In total, the amount of Γ_7 is thought to be nearly equal for both the 1*k* and 3*k* structures. An interesting question is whether the present model can explain the anomalous transport properties, particularly the strong increase in the electrical resistivity in the 3*k* structure compared with the 1*k* structure, indicating the characteristics of low carrier density. This situation is shown schematically in Fig. 6 [39]. In the paramagnetic state, the electrical resistivities in USb, a typical material to show the 3*k* structure below $T_N = 213$ K, and that in UAs, a typical material to show the 1*k* structure below $T_N = 124$ K and furthermore to change to the 2*k* structure below 62 K, are similar in terms of both absolute value and temperature dependence to those of CeP and CeAs as shown in Fig. 7, indicating characteristic behavior for low carrier density systems similar to CeXp. Below the ordering temperature, the resistivity in UAs decreases in the usual way, indicating that the change in the carrier number is minor. In USb, however, the resistivity increases sharply below the ordering temperature and decreases finally at low temperature giving rise to a large peak, similar to the c-axis resistivity in the heavy rare earth metals mentioned before, in which the carriers at the nesting Fermi surface are lost below the ordering temperature. Judging from the large peak of resistivity, the lost carriers in USb are in a much larger ratio than in the heavy rare earth metals. These characteristic behaviors are explained as follows. The Brillouin zones for the 1*k* and 3*k* type I structures are shown in Fig. 8. The volume of the Brillouin zone is reduced to one-half and one-quarter that of the initial one respectively. For the 1*k* structure, the same situation as in CeXp is expected and the doubly degenerated p–f antibonding band appears along the Γ–X_z axis. The carrier number is also expected to be similar to that in CeSb, at most 0.1 per U. For the 3*k* structure, the doubly degenerated p–f antibonding band appears on all the three Γ–X axes, occupying a fairly large area of the reduced Brillouin zone. Because the three X-

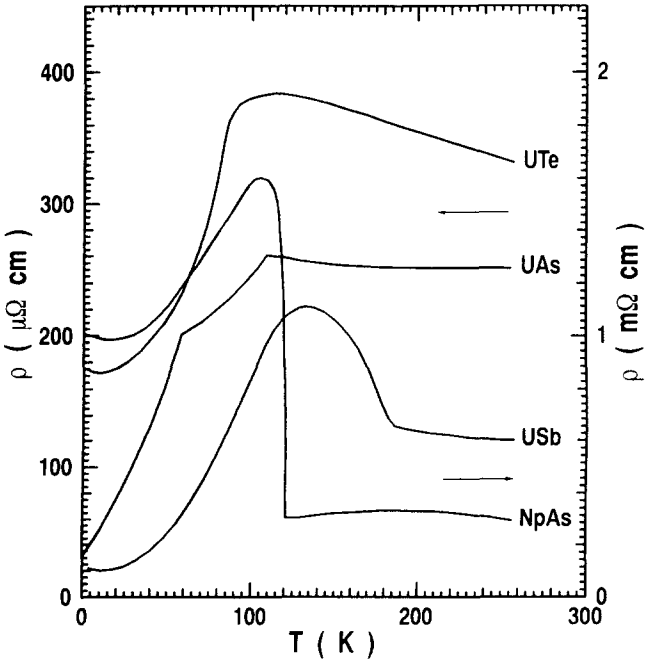

Fig. 6. Schematic picture for the electrical resistivity ρ of various U-compounds as functions of temperature T. Note the different scales for ρ as indicated by the arrows.

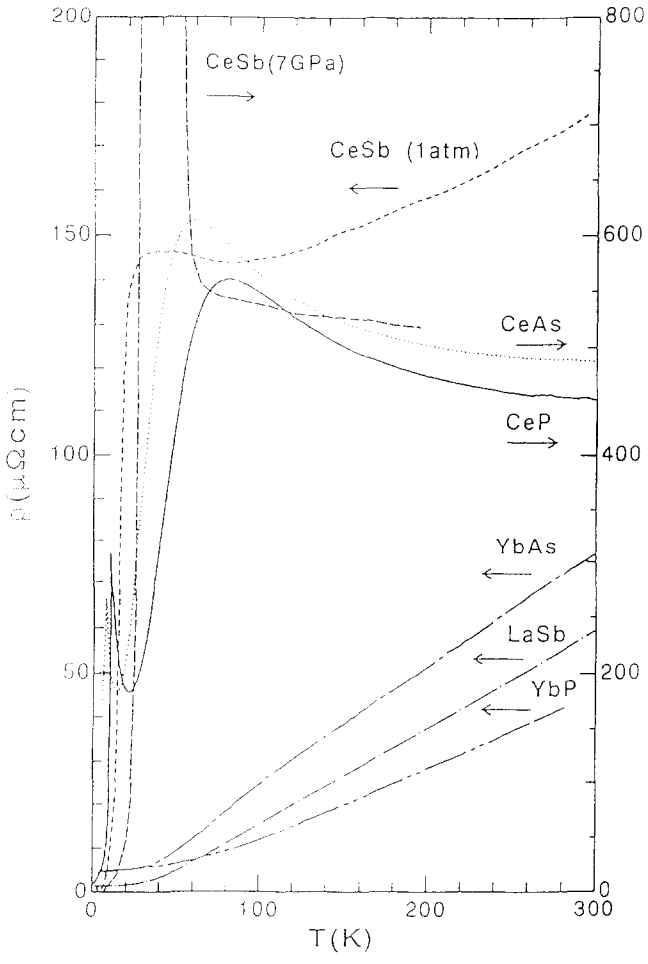

Fig. 7. Electrical resistivities ρ for various rare earth monopnictides as functions of temperature T. Note the different scales for ρ as indicated by the arrows. All data are at 1 atm except CeSb (7GPa), in which the maximum value of ρ is 2.6 mΩ cm at 35 K.

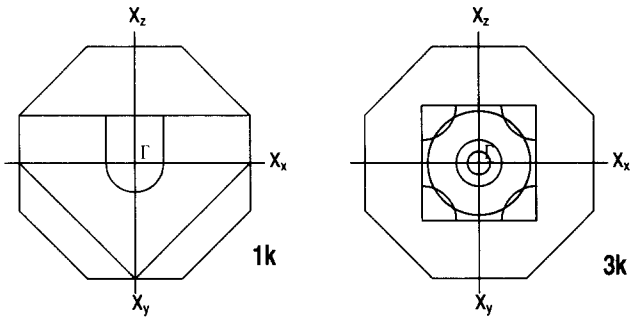

Fig. 8. The initial and the reduced Brillouin zones for the 1*k* and the 3*k* type I orderings are shown as the outer and inner boundaries. For the 1*k* structure, the large hole surface corresponding to the β_4 branch in Fig. 2 is shown schematically. In CeSb for the ferromagnetic state shown in Fig. 1, this Fermi surface extends nearly to the boundary X_z in the initial Brillouin zone. For the 3*k* structure, a schematic picture for the electron and hole Fermi surfaces are shown without mixing between them. When the mixing between them is introduced, the large electron and hole Fermi surfaces are cancelled out strongly leaving small hole surfaces.

points are folded onto the Γ-point, the bottom of the conduction band is at the Γ-point with sixfold degeneracy for the t_{2g} symmetry. Therefore, three kinds of spherical bands appear around the Γ-point. Of these, two have small effective masses and one has a fairly large mass corresponding to the usual *d* band as seen in Fig. 1, and the last one mixes strongly with the p–f antibonding band near the Fermi energy destroying the main part of their Fermi surfaces. Therefore, we have small electron Fermi surfaces around the Γ-point with small effective masses and small hole surfaces near the corner of the Brillouin zone. Therefore, the carrier number is much smaller than that for the 1*k* structure and, because the effective mass of electron is small, the impurity effect is not strong even for the low carrier density system. The Hall constant changes sign from positive at the paramagnetic region to negative at low temperatures in the ordered region. These changes are indeed consistent with the present picture. Note that some amount of positive anomalous Hall effect is seen in the paramagnetic region, but rapidly decreases in the ordered region. The carrier number estimated from the Hall constant at the lowest temperature assuming no contribution from the holes is about 0.015 U^{-1}, indicating that the real carrier number is on the order of 1% per U-atom. This is consistent with the recently measured dHvA result [41].

The next question is whether the magnetic polaron liquid is formed in the paramagnetic region or not. The answer is positive because the behavior of resistivity is very similar to that of CeP and CeAs. The existence of a magnetic polaron liquid in CeP and CeAs was deduced from Fig. 7 as follows [42]. Except at low temperature, the carrier number is nearly equal in all of the materials in Fig. 7, that is, from 0.02 to 0.04 per R-atom. No Kondo scattering and no magnetic polaron liquid are observed in YbXp at high temperature and the resistivity is essentially the same as that in LaXp, indicating normal magnetic scattering. As mentioned before, the Γ_8 Kondo scattering dominates at high temperature in CeSb, causing the characteristic temperature dependence. In CeP and CeAs, as well as in CeSb under applied pressure, the resistivity is four times larger than that in CeSb at ambient pressure. Such a large scattering is not expected from Kondo scattering, but is consistent with the magnetic polaron liquid with a giant moment, which causes strong scattering proportional to the square of the giant moment. The increase in resistivity for decreasing temperature is due to the stronger moment at lower temperature. For the same reason as above, we expect the same magnetic polaron liquid formation in UXp. This is actually very natural because of the stronger p–f mixing interaction in UXp, which should cause a stronger magnetic polaron effect. The carrier number is expected to be similar to those in CeSb and CeBi.

It is important to notice that NpXp has very similar characteristics to UXp. This confirms our argument that, instead of the conventional 5f band model, the URHF bands with $5f^3$ and $5f^4$ occupations for UXp and NpXp respectively should be applied. In this case, in the paramagnetic region, we have a similar semimetallic behavior to that in CeXp. In the 3*k* structure in NpXp, one additional 5f state with Γ_7-like character of a small moment is expected to sit below the Fermi energy and enhances the magnetic character. Otherwise, the same situation as in UXp exists, as shown in Fig. 6 for NpAs as an example. This compound orders at 175 K in a 1*k* type structure. However, the resistivity changes only slightly. At 140 K. the 3*k* type I structure appears and then the resistivity increases very strongly, much more so than in USb. The carrier number is estimated to be similar to that in CeAs at low temperature and thus the impurity effect is also strong. This is clearly due to the stronger p–f mixing effect caused by the larger 5f moment.

Now UXc compounds are treated briefly. They order ferromagnetically with the moment along the [111] direction, definitely different from UXp. However, the resistivity at high temperature is similar to those for UXp, suggesting low carrier density systems with the magnetic polaron liquid. This is definitely different from CeXc, which are monovalent metals with trivalent Ce, showing the Kondo behavior in CeTe. These facts clearly indicate the following picture for UXc. In UXc, U should be treated as tetravalent, in the same sense as in the Ce-compounds in the valence fluctuation regime, and thus the case for CeN mentioned before. This is essential for the application of the Luttinger theorem and thus indicates that UXc are divalent metals or semimetals when the first doubly occupied conduction bands are nearly filled. Indeed, the latter condition is

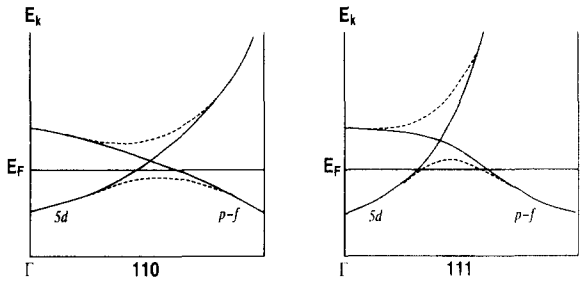

Fig. 9. Schematic pictures for the dispersions of the 5d and the p–f antibonding bands along the (110) and (111) directions for the ferromagnetic ordering with the magnetic moment along (111). The dotted curves indicate the result with the mixing interaction between them. The position of the Fermi energy is shown by the solid lines labeled E_F.

nearly satisfied and the semimetallic character can be deduced by the following consideration. To accommodate two electrons per U-atom in the conduction bands, the Fermi energy should be slightly above the 5d t_{2g} band states at the Γ-point, as shown in Fig. 1. Conversely, two occupied 5f states should be of the Γ_7-like states with weak p–f mixing interaction. The Γ_8-like 5f states are in principle above the Fermi energy. However, because the p–f mixing is strong around the Γ-point but becomes weak as the wave vector deviates from the Γ-point as mentioned before, we obtain the dispersion as shown in Fig. 9, and thus some part becomes below the Fermi energy. Then, the mixing between the 5d band and the p–f antibonding band erases the greater part of the electron and hole Fermi surfaces leaving small semimetallic electron and hole Fermi surfaces at around the Γ-point and the corner of the Brillouin zone with the hole surface between them. Because of the above situation, the p–f mixing for the occupied 5f states is weak but that for the unoccupied 5f states is strong and thus the average population of the 5f states increases, in the same sense as in the Ce-compounds in the valence fluctuation regimes, causing the average 5f population to be near 3.

5. Discussion and conclusions

The fundamental characteristics of the electronic states in the U-compounds in the anomalous heavy fermion regime have been studied by applying the ideas clarified in the anomalous rare earth compounds, as well as in the transition metal compounds. It was shown that the unrestricted Hartree–Fock band picture similar to that employed in the Ce-compounds in the Kondo regime, in particular Ce-monopnictides, is the appropriate starting model to understand the anomalous U-compounds. In the usual band calculation for Fe and Ni, only the spin split band is obtained due to the approximation of the local density potential. To calculate the magnon dispersion correctly, however, the orbital states should be treated correctly in the sense of the tight binding model, which naturally causes the URHF-like state. Based on this standpoint, unusual magnetic and transport properties in U-monopnictides and monochalcogenides were studied, and it was shown that fundamentally their anomalous properties can be understood through this model. In U-monopnictides, the 1*k* magnetic ordering is essentially through the same mechanism as in Ce-monopnictides in which the 4f state of full moment along the z-axis mixes strongly with the p-states on the nearest neighbor pnictogen atoms on the xy-plane causing the largest gain of the p–f mixing energy. In this case, the positive non-linear effect plays an essential role. Two occupied Γ_7 type 5f states are more remote from the Fermi energy. When the magnetic moment in U increases, the positive non-linear effect now turns into the negative non-linear effect because of the stronger p–f mixing interaction and then the 3*k* magnetic ordering is stabilized with the 2*k* structure in the intermediate state, in which the total magnetic moment is divided into three components, or two components. Then, at each site, the total magnetic moment is directed into one of the [111]-like directions, or [110]-like directions. A natural question is why a 1*k* structure with the moment along the [111] direction is not found. The answer is that, even if we start from the 1*k* type with the moment along [111], the 3*k* type structure is obtained to maximize the p–f mixing effect. The energy difference between them is thought to be small and indeed the ferromagnetic ordering in U-monochalcogenides corresponds to such a structure, in which the Γ_8 valence bands mix in the three x, y and z directions with the 5fΓ_8 states causing holes on the antibonding p–f mixing band along the three principal axes. It is also shown that the similarity in behavior of Np-monopnictides with U-monopnictides is naturally explained in the present URHF model, in which An atoms are treated as trivalent. On the other hand, in An-monochalcogenides, An should be treated as tetravalent, similar to the valence fluctuation regime in the Ce-compounds. In this case, semimetallic behavior is naturally obtained. The strong decrease in the carrier number in the 3*k* magnetic ordering is also explained naturally.

In the Ce-compounds, we discussed the difference between the Kondo regime and valence fluctuation regimes as due to the splitting of the 4f state in the sense of the unrestricted Hartree–Fock model. Anomalous heavy fermion character appears mostly in the former regime, even though some materials near the border in the latter regime also show anomalies. In the anomalous heavy fermion U-compounds, we applied the same idea. However, because U_f is small in the U-compounds in general, the energy splitting is small and

thus the difference between the unrestricted Hartree–Fock and the usual one is not clear compared with the Ce-compounds in the Kondo regime. Recently, it was found that in $CeRu_2Si_2$ the two regimes can change continuously with applied magnetic field [43]. Therefore, in the U-compounds, such a continuous change may be easier. The Luttinger theorem is expected to work accurately within each regime. Smooth crossover is possible when the quasi particles for one regime fade out and those for another regime appear continuously. More studies are definitely needed to confirm such a picture.

In Ce-monopnictides, the Γ_8 magnetic polaron liquid state is stabilized even at room temperature, supported by the long-range Coulomb repulsive force characteristic for the low carrier density systems. Because of the stronger p–f mixing interaction, we naturally expect such a state in both An-monopnictides and An-monochalcogenides. Indeed, the absolute value and the temperature dependence in the paramagnetic region are very similar to those in CeP and CeAs, which are typical magnetic polaron liquid systems. It is important to notice that many other U-compounds show similar behavior, which is usually attributed, without proof, to the Kondo effect. It should be noted, however, that because of the small 5f–5f correlation energy the typical Kondo state is difficult to form in the U-compounds. This point is discussed in detail in Section 2, together with the fact that there is no antibonding Kondo peak in the photoemission spectra in the U-compounds. In this sense, the Kondo-like temperature dependence of resistivity in the U-compounds may be better attributed to the magnetic polaron liquid state. Indeed, the absolute value of resistivity in such materials is usually much higher than that of the typical Kondo systems in the Ce-compounds. More studies are also necessary to confirm this point.

Acknowledgements

The main part of this paper was written when the author was staying in CEN in Grenoble in the summer of 1994. The author would like to express his cordial thanks to J. Flouquet, L.P. Regnault, P. Burlet and D. Braithwaite for their hospitality and valuable comments and help with the present paper.

References

[1] T. Kasuya, *Prog. Theor. Phys., 16* (1955) 45, 58.
[2] T. Kasuya, in G.T. Rado and H. Suhl (eds.), *Magnetism IIB*, Academic Press, New York, 1966, p. 215.
[3] T. Kasuya, *J. Alloys Compos., 192* (1993) 11, 217 and references therein.
T. Kasuya, *J. Appl. Phys.*, to be published, and references therein.
[4] T. Penney, F. Holtzberg, L.J. Tao and S. von Molnar, *AIP Conf. Proc., 18* (1974) 980.
[5] T. Kasuya, *IBM J. Res. Dev., 14* (1970) 214.
[6] T. Kasuya, *CRC Crit. Rev., Solid State Sci., 3* (1972) 131.
[7] O. Sakai, A. Yanase and T. Kasuya, *J. Phys. Soc. Jpn., 42* (1977) 596.
[8] K. Takegahara and T. Kasuya, *J. Phys. Soc. Jpn., 39* (1975) 1292, and references therein.
[9] T. Kasuya, A. Yanase and T. Takeda, *Solid State Commun., 8* (1970) 1551.
T. Kasuya, *Solid State Commun., 8* (1970) 1635.
[10] M. Umehara and T. Kasuya, *J. Phys. Soc. Jpn., 40* (1976) 340 and references therein.
[11] S. von Molnar and T. Kasuya, in S.P. Keller, J.C. Hensel and F. Stern (eds.), *Proc. 10th Int. Conf. Physics Semiconductors*, p. 233.
[12] O. Sakai, Y. Shimizu and T. Kasuya, *Prog. Theor. Phys., Suppl., 108* (1992) 73 and references therein.
[13] C.S. Wang and J. Callaway, *Phys. Rev., B15* (1977) 298.
[14] J.F. Cook, *Phys. Rev., B7* (1973) 1108.
[15] D.E. Eastman, F.J. Janak, A.R. Williams, R.V. Coleman and G. Wendin, *J. Appl. Phys., 50* (1979) 7423.
J. Kübler and V. Egert, in K.H.J. Buschow (ed.), *Materials Science Technology*, Vol. 3A, Part I, VCH, Weinheim, 1992, p. 3.
[16] T. Kasuya, *Proc. Memorial Symposium for J. Rossat-Mignod* (1994), to be published.
[17] S. Suzuki *et al., Jpn. J. Appl. Phys. Ser., 8* (1993) 59.
T. Ishii, *Physica, B186-188* (1993) 21.
[18] Y. Onuki, T. Goto and T. Kasuya, in K.H.J. Buschow (ed.), *Materials Science and Technology*, Vol. 3A, Part I, VCH, Weinheim, 1992, p. 545.
T. Kasuya, *Jpn. J. Appl. Phys. Ser., 8* (1993) 1.
T. Kasuya, *Prog. Theor. Phys. Suppl., 108* (1992) 1.
[19] O. Sakai, M. Takeshige, H. Harima, K. Otaki and T. Kasuya, *J. Magn. Magn. Mater., 52* (1985) 18.
[20] T. Kasuya, *Proc. Memorial Symposium for J. Rossat-Mignod*, to be published.
[21] J.M. Luttinger, *Phys. Rev., 119* (1960) 1153.
[22] T. Kasuya in T. Kasuya and T. Saso (eds.), *Theory of Heavy Fermions and Valence Fluctuations*, Springer-Verlag, Berlin, 1985, p. 2.
[23] M. Takeshige, O. Sakai and T. Kasuya, *J. Phys. Soc. Jpn., 60* (1991) 666.
M. Takeshige, R. Takayama, O. Sakai and T. Kasuya, *Jpn. J. Appl. Phys. Ser., 8* (1993) 129.
[24] S. Hüfner and G.K. Wertheim, *Phys. Lett., A51* (1975) 299.
[25] T. Kasuya, *Physica, C223* (1994) 223.
[26] T. Kasuya, *Physica, C224* (1994) 191.
[27] T. Kasuya, A. Oyamada, M. Sera, Y. Haga and T. Suzuki, *Physica, B199 & 200* (1994) 585 and references therein.
[28] T. Kasuya, Y. Haga, T. Suzuki, Y. Kaneta and O. Sakai, *J. Phys. Soc. Jpn., 61* (1992) 3447.
[29] T. Kasuya, T. Suzuki and Y. Haga, *J. Phys. Soc. Jpn., 62* (1993) 2549.
[30] T. Kasuya, Y. Haga, T. Suzuki, T. Osakabe and M. Kohgi, *J. Phys. Soc. Jpn., 62* (1993) 3376.
[31] M. Kohgi, T. Osakabe, K. Kakurai, T. Suzuki, Y. Haga and T. Kasuya, *Phys. Rev., B49* (1994) 7068.
[32] T. Kasuya, Y. Haga and T. Suzuki, in *Proc. Int. Conf. on Transition Metal Compounds*, Wroclaw, Poland, 1994, to be published.

[33] T. Kasuya, M. Sera and T. Suzuki, *J. Phys. Soc. Jpn., 62* (1993) 3364.
[34] T. Kasuya, *Europhys. Lett., 26* (1994) 227.
[35] T. Kasuay, *Europhys. Lett., 26* (1994) 283.
[36] J.M. Imer, D. Malterre, M. Grioni, P. Weibel and Y. Baer, *Phys. Rev., B44* (1991) 10455.
[37] F. Patthey, B. Delley, W.D. Schneider and Y. Baer, *Phys. Rev. Lett., 55* (1985) 1518.
[38] G.H. Lander, 1994.
[39] J.M. Fournier and Gratz, 1994.
[40] M. Sera, T. Fujita, T. Suzuki and T. Kasuya, in P. Wachter and H. Boppart (eds.), *Valence Instabilities,* North Holland, 1982, p. 435.
[41] A. Ochiai, personal communication.
[42] T. Kasuya, Y. Haga, Y.S. Kwon and T. Suzuki, *Physica B186–188* (1993) 9.
[43] Y. Ônuki, personal communication.